Modelling the Effect of Lithium on SOL Dynamics and the SOL Heat Flux Width Observed in NSTX*

D.A. Russell[1], D.A. D'Ippolito[1], J.R. Myra[1], J.M. Canik[2], T.K. Gray[2], S.J. Zweben[3]

[1]Lodestar Research Corporation, Boulder, CO, USA
[2]Oak Ridge National Laboratory, Oak Ridge, TN, USA
[3]Princeton Plasma Physics Laboratory, Princeton, NJ, USA

E-mail contact of main author: dave@lodestar.com

Abstract. The effect of lithium (Li) wall coatings on scrape-off-layer (SOL) turbulence in NSTX is modeled with the Lodestar SOLT code. Specifically, the implications for the SOL heat flux width of experimentally observed, Li-induced changes in the pedestal profiles are considered. The connection is important because pedestal profiles impact the overall fusion performance of ITER and future machines while the SOL heat flux width impacts the survivability of divertor target plates. The SOLT code used in the modeling has been expanded recently to include ion temperature evolution and ion diamagnetic drift effects. This work focuses on two NSTX shots occurring pre- and post-Li deposition. The simulation density and energy profiles are constrained, inside the last closed flux surface *only*, to match those measured in the two experiments, and the resulting drift-interchange-driven turbulence is explored. The effect of Li enters the simulation only through the pedestal profile constraint: Li modifies the experimental density and temperature profiles, and these profiles affect the simulated SOL turbulence. The power entering the SOL (P_{SOL}) measured in the experiments is matched in the simulations by adjusting "free" dissipation parameters (e.g., diffusion coefficients) that are not measured directly in the experiments. At power-matching, (a) the heat flux SOL width (λ) is smaller in the case with Li, as observed experimentally, and (b) density fluctuation amplitudes are reduced, with Li, also as observed. The instabilities and saturation mechanisms that underlie the SOLT model equilibria are discussed.

* Work supported by USDOE grants DE-FG02-97ER54392 and DE-FG02-02ER54678.

1. Introduction

It has been established that lithium (Li) wall conditioning improves tokamak performance. With lithium deposition on plasma-facing components (PFCs) in the National Spherical Torus Experiment (NSTX), observed improvements include increases in electron and ion temperature, increases in energy confinement times and reduced magneto-hydrodynamic turbulence[1] including the suppression of edge-localized modes (ELMs).[2] It is generally believed that lithium coating provides improved performance through reduced ion (deuterium) recycling and high-Z impurity control at the PFCs. However, predictive models of the interplay between plasma edge conditions and recycling dynamics are scarce, and the origins of improved confinement in lithium deposition is a topic of on-going investigation.

In a series of discharges in NSTX,[3,4] electron density and pressure profiles in the edge pedestal region relaxed (i.e., profile gradients decreased) significantly (~100%) with increasing lithium deposition. Along with the profile relaxation, reduced recycling, decreased electron transport and ELM suppression were observed. ELM suppression was attributed to the reduced drive of magneto-hydrodynamic instabilities (peeling-ballooning modes) that comes with reduced pressure gradients in the edge region. A reduction in the intensity of the deuterium alpha-line emission (D_α), measured at the lower divertor in these discharges, is particularly noteworthy, in the context of this paper, as it points to a possible reduction in turbulent transport across the separatrix. It has been observed by infrared thermography (IRTV) that lithium deposition

reduces both the radial heat flux ($q_\perp$) and the heat flux width, λ, at the divertor and so, by magnetic field line mapping, reduces λ in the outboard midplane (OM) in NSTX.[5]

Interpretative transport studies[6] of two of the NSTX discharges, one with and one without lithium coated PFCs, concluded that a decrease of ~75% in the particle and energy transport coefficients, D and χ_e, was consistent with the observed profile relaxation with lithium deposition. That calculation was based on a diffusive transport model inside the separatrix and did not include a contribution from turbulent convection. Yet, the same study provides evidence that lithium decreases turbulent fluctuations in the edge and SOL. Edge reflectometry measurements suggest normalized density fluctuations ($\delta n/n$) of ~10% in the pre-Li case and ~1% in the with-Li case, near the separatrix, with the pre-Li value approaching unity in the near-SOL. Thus further investigation of the effects of lithium on turbulent transport is well motivated.

In the present study, we model turbulent transport in two NSTX discharges, one with and one without lithium, using a newly updated version of the SOLT code. This approach was motivated by previous successful studies of the SOL heat-flux width in low-power H-mode discharges in NSTX[7] and of an EDA H-mode in Alcator C-Mod.[8] As in those studies, we focus on the heat-flux width at power-matching with the experiments. It is demonstrated that the observed reduction in heat-flux width in the experiments corresponds to the reduction in interchange-driven turbulent transport, in the model simulations, that results from the gentler pressure profiles associated with lithium deposition.

The rest of the paper is organized as follows. The newly updated SOLT model equations, which now include the self-consistent evolution of the ion pressure and ion diamagnetic drift, are presented in Section 2. Section 3 describes the input to SOLT from the experiments, the method of matching the power crossing the separatrix (P_{SOL}) with the experiments, and the power-matched heat flux widths. Section 4 discusses the mean flows observed in the simulations. Gas-puff imaging (GPI) data provides information on flow velocities in NSTX. To enable comparison with GPI data, we introduce a structure velocity diagnostic for the simulations and demonstrate its dependence on flow damping. Section 5 presents conclusions.

2. Model Equations

SOLT is a two-dimensional (2D) electrostatic fluid turbulence code. The code models the evolution of potential, density and temperature in a plane perpendicular to the magnetic field B, in the outboard midplane (OM) region of the torus. The potential evolution is obtained from the evolution of the generalized vorticity. SOLT contains a reduced description of the electron drift wave and interchange instabilities, and sheath physics. Curvature- and grad-B-driven charge polarization enables transport of enhanced density structures (blobs) with strong fluctuations ($\delta n/n \sim 1$) from the edge into the SOL. The parallel physics is modeled by closure schemes that depend upon the regime.[9] The code has recently been generalized to allow regime-dependent closures for the parallel current and heat flux.

In dimensionless form, the SOLT model equations of evolution are

$$(\partial_t + v_E \cdot \nabla)\rho = -2b\times\kappa\cdot\nabla(p_e + p_i) - J_{//} + \mu\nabla^2\rho - \nu_{\bar{\rho}}\bar{\rho} + \tag{1}$$

$$+\frac{1}{2}\left[nv_{di}\cdot\nabla\nabla^2\phi\right] - \frac{1}{2}\left[v_E\cdot\nabla(\nabla^2 p_i) - \nabla^2(v_E\cdot\nabla p_i)\right] - \frac{1}{2}b\times\nabla n\cdot\nabla v_E^2$$

$$(\partial_t + v_E \cdot \nabla)n = -J_{//e} + D_n\nabla^2 n + S_n \tag{2}$$

$$(\partial_t + v_E \cdot \nabla)T_e = -q_{//e}/n + D_{Te}\nabla^2 T_e + S_{Te} \tag{3}$$

$$(\partial_t + v_E \cdot \nabla)T_i = -q_{//i}/n + D_{Ti}\nabla^2 T_i + S_{Ti} \tag{4}$$

where the generalized vorticity ρ evolved in Eq. (1) is defined by

$$\rho + \nabla\cdot(n\nabla\phi + \nabla p_i) = 0\,. \tag{5}$$

The equations are written in dimensionless form using Bohm normalization with reference time-scale $\Omega_{ci}^{-1} = (ZeB/m_ic)^{-1}$ and space-scale $\rho_{sr} = c_{sr}/\Omega_{ci}$, where $c_{sr}^2 = T_{er}/m_i$, and T_{er} is a reference temperature for the normalization. ϕ is the electrostatic potential, n is the electron density, $T_{e,i}$ are the electron and ion temperatures, and $p_{e,i} = nT_{e,i}$ are the corresponding pressures. The ExB velocity is $v_E = b\times\nabla\phi$, where b is a unit vector in the magnetic field direction, perpendicular to the plane of the simulations. The ion diamagnetic drift velocity is $v_{di} = b\times\nabla p_i/n$.

Zero-order gradients of the profiles are in the x (radial) dimension in the simulations. The core-side boundary is at x = 0, and the separatrix is at x = Lx/2 with the far-SOL boundary at x = Lx. All fluctuations (δn, etc.) vanish at the x-boundaries. The turbulence is homogeneous in the y (bi-orthogonal, approximately poloidal) dimension where periodic boundary conditions are applied. The over-bar, e.g. $\bar{\rho}$ in (1), denotes the y-average or mean.

This edition of the SOLT model differs from previous ones in that it evolves the ion temperature and the generalized vorticity (5), thus dynamically coupling the ion diamagnetic and ExB drifts. The vorticity evolution (1) is consistent with the drift-ordered, reduced-Braginskii fluid model version derived by Simakov and Catto[10] and is used in the BOUT code.[11] In Eq. (1), the damping of the mean vorticity ($\sim\nu_{\bar{\rho}}\bar{\rho}$) provides mean flow damping, by charge-exchange with neutrals, for example. Note that $\rho = 0$ corresponds to $v_E = -v_{di}$ and that, to lowest order, flow damping encourages $\bar{v}_{E,y} = -\bar{v}_{di,y}$.

The other new terms in Eq. (1), that vanish in the limit of zero ion pressure, provide finite Larmour radius (FLR) stabilization, for example, and allow for the ion temperature gradient instability, though the latter is insignificant in this study. The last term originates in the convective derivative, $v_E\cdot\nabla$, acting on $\nabla\cdot(n\nabla\phi)$ in the generalized vorticity. It is important for describing the Kelvin-Helmholtz (K-H) instability in the presence of a density gradient, for example.

The curvature and grad-B forces combine in the first term ($\sim \kappa \equiv \mathbf{b}\cdot\nabla\mathbf{b}$) on the right-hand side of Eq. (1) to drive the interchange instability. In our coordinate system, this term is simply $\beta\cdot\partial_y(p_e + p_i)$, where $\beta = 2\rho_{sr}/R$ and R is the radius of curvature of the magnetic field ($1/\kappa$), here approximated by the major radius of the tokamak. The linearized equations recover the interchange growth rate, $\gamma^2_{mhd} = -\beta\,\partial_x(p_e + p_i)/n$, now including the ion pressure contribution.

Explicit diffusion coefficients are μ, D_n, D_{Te}, and D_{Ti}. These describe diffusive transport processes in addition to that generated self-consistently by interchange turbulence. As it is difficult to extract appropriate values for these coefficients from experimental data, we regard them as "free" parameters and adjust them to achieve physically credible results: they should dissipate the high-k turbulence but not be so large as to dominate the SOL heat flux width or turn off instability. In Sec. 3, we describe adjusting the density diffusion coefficient D_n to tune the power P_{SOL} in the simulations to match that observed in the experiments.

The sources, S_n, S_{Te}, and S_{Ti}, have the form $S_n = \nu_n\cdot(n_0(x) - n)$, etc., which tends to restore the reference profiles ($n_0(x)$, etc.) taken from the experiments. The sources are non-zero only inside the separatrix; evolution in the SOL is source-free. These may be thought of as maintaining profiles against fluctuations, born in the outboard midplane, with plasma that streams in and out of the midplane region along the closed field lines.

The current densities ($J_{//}$, $J_{//e}$) and heat fluxes ($q_{//e}$, $q_{//i}$) in Eqs. (1-4) close the system of equations when expressed in terms of ϕ, n, T_e and T_i. Those closure relations, valid for a range of collisionality regimes, from conduction-limited (at high collisionality) to sheath-connected, are discussed in a paper that directly motivates the present work.[7] (Expressions given there are slightly modified to include the ion temperature in present work.) We emphasize that the current and heat flux adjust continuously between sheath- and conduction-limited expressions in the SOL as the fields evolve, depending self-consistently on the character of the turbulence.

3. SOLT Simulations

3.1 Input to SOLT from the Experiments

The parameters and profiles for the simulations are taken from two discharges in NSTX: one without lithium, or "pre-Li", #129015, and one with lithium, or "with-Li", #129038. These discharges are described in Ref. [6] and are two of a series exploring edge turbulence reduction resulting from lithium deposition to plasma-facing components. Both shots were 0.8 MA H-modes driven by neutral beam injection (NBI). The pre-Li shot was driven with 3.9 MW NBI, and the with-Li shot with 2 MW NBI. Despite the discrepancy in injected power, the stored energy was the same in both shots due to the improved energy confinement that comes with lithium deposition. We fit the density and temperature profiles measured in the experiments

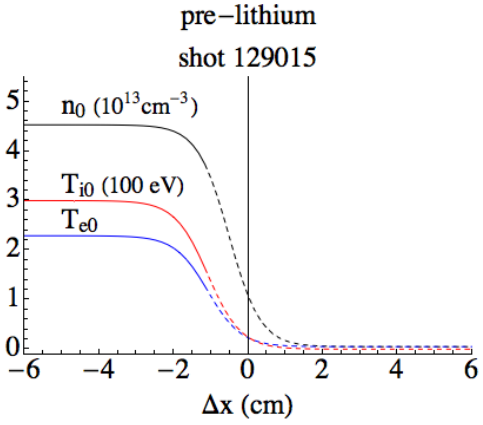

FIG. 1. Reference profiles of density and temperature, relative to the separatrix, for the pre-Li discharge.

with hyperbolic tangent functions, as illustrated in Fig. 1. Simulation profiles relax to these *on the core side of the separatrix* ($\Delta x < 0$) *only*, at rates that vanish monotonically as $\Delta x \rightarrow 0^{(-)}$. The dashed lines in the figure indicate that the density and temperatures are increasingly free to evolve as the separatrix is approached and totally unconstrained in the SOL.

The currents ($J_{//}$, $J_{//e}$) and heat fluxes ($q_{//e}$, $q_{//i}$) in Eqs. (1-4) are functions of the turbulence (ϕ, n, T_e and T_i) that depend on the fixed parameters of the experiment through coefficients.7 For example, the "sheath coefficient" is the inverse connection length, from the OM to the divertor sheath in the SOL. The sheath tends to dominate parallel transport in the SOL as the connection length decreases. The reference parameters for both the pre-Li and with-Li shots are T_{er} = 100 eV, c_{sr} = 69.2 km/s, $\Omega_i / 2\pi$ = 25.7 MHz (B_{OM} = 3416 G), $\rho_{sr} = c_{sr} / \Omega_i$ = 4.23 mm, and the reference density is 10^{13} cm^{-3}; both are deuterium plasmas.

3.2 Matching P_{SOL} to the Experiments

SOLT's turbulence (e.g., P_{SOL} and λ) depends on physical parameters for which experimental values are not available *a priori*, particularly the dissipation parameters μ, ν_ρ, D_n, D_{Te} and D_{Ti}. For reasonable choices of these parameters, the simulations recover some of the experimental observations. For example, the diffusion of density D_n can be adjusted to recover the observed power. See Fig. 2. In the figure, the circles indicate the measured values of P_{SOL}: 3.9 MW in the pre-Li discharge and 2.0 MW in the with-Li discharge. The corresponding density fluctuations confirm that the drift-interchange-driven turbulence is weaker for the smaller pressure-gradients of the pedestal with lithium and stronger for the steeper pre-Li profiles. Density fluctuations at the separatrix are weaker across the wave-number spectrum in the with-Li case, in qualitative agreement with reflectometry measurements.[12] *Turbulent (blob) heat transport is weaker for the broader profiles with lithium.*

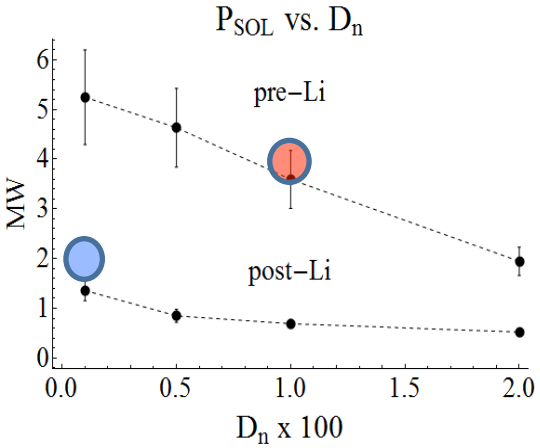

Fig. 2. P_{SOL} from SOLT simulations vs. density diffusion coefficient D_n. Large circles indicate experimental values.

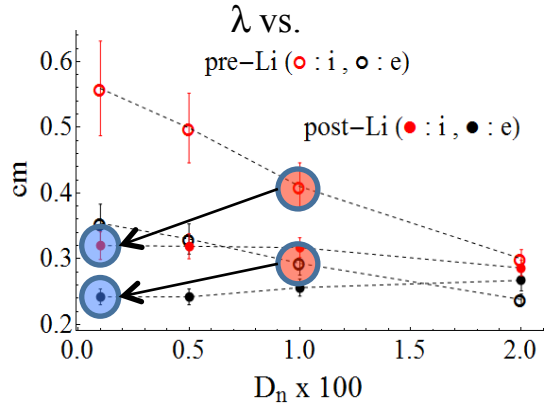

At power matching, the heat flux profile width in the SOL (λ) is *smaller* in the with-Li simulation, consistent with the trend observed in experiments, indicated with arrows in Fig. 3. As seen in the figure, particularly in the pre-Li case, the width decreases with increasing diffusion coefficient, D_n. If diffusion were driving the heat flux, one would expect λ to increase with increasing D_n, but

the opposite is observed in the simulations; *the turbulence drives the heat flux and the diffusion damps the turbulence*.

FIG. 3. Heat-flux profile width in the SOL $\lambda = P_{SOL} / [q_{//}(\Delta x \to 0^{(+)}) \cdot 2\pi RB_\theta / B]$ *vs.* D_n *for electrons (black) and ions (red) in the pre-Li (circles) and with-Li (disks) cases. Larger circles indicate power-matching, cf. Fig. 2.*

4. Mean Flows in SOLT Turbulence

Sheared mean flows reduce the interchange growth rate and act as transport barriers in the edge region. To the extent that the heat flux width is determined by turbulent transport, as here, it is important to explore the mean flows in the simulations and to compare them with those observed in the experiments. If the flows can be adjusted in the simulation by tuning parameters accessible in the experiments, it would have important implications for controlling the turbulent transport and the heat flux width.

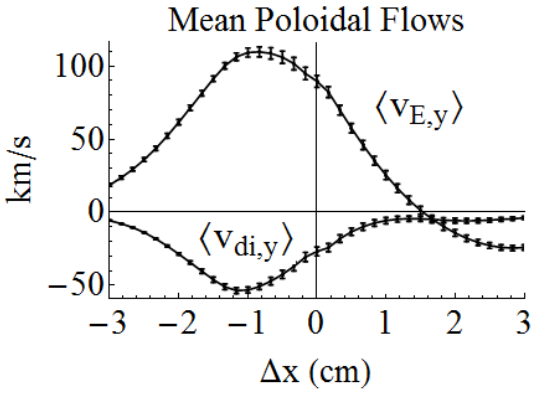

FIG. 4. Poloidal ExB and ion diamagnetic drift velocities averaged over the poloidal dimension (y) and time for the power-matched pre-Li simulation. Error bars are standard deviations.

The time-averaged mean poloidal flow, $\langle v_{E,y} \rangle$ for the power-matched, pre-Li simulation is shown in Fig. 4. The shape of the profile is generic for these simulations: a near-sonic, positive maximum (in the electron diamagnetic drift direction) inside the separatrix, with flow reversal in the SOL where the sheath enforces the Bohm potential ($3T_e$) and consequent negative (ion diamagnetic direction) flow. Thus there are flow shear layers, $\partial_x \langle v_{E,y} \rangle$, on either side of the high pressure gradient region, where the ion diamagnetic drift, $\langle v_{di,y} \rangle$, also plotted in Fig. 4, has a negative global minimum. Are similar flows present in the experiment?

The maximum magnitude of $\langle v_{E,y} \rangle$ is much larger than the poloidal turbulent structure (blob) velocities observed near the separatrix with GPI on NSTX.[13] But, are the SOLT and experimental *mean flow velocities* so dissimilar? How do blobs move in the background flow? To explore these questions, we introduce a synthetic structure velocity for the simulations.

Near the separatrix, blob density tracks in (y,t) space show up as strong linear features in the power spectrum of the density fluctuations. At each radial location (Δx), we define the *structure velocity* to be the phase velocity at the global maximum of the power spectrum, $|\delta n(\Delta x, k_y, \omega)|^2$. When this velocity is plotted as a function of Δx, it is seen to be constant on radial intervals. One such interval includes the pedestal region and overlaps the separatrix, extending into the near-SOL, while another starts near the flow-reversal point and extends into the far-SOL. See Fig. 4. Linear analysis of the equilibrium, time-averaged turbulence profiles reveals distinct normal modes localized to these radial zones, viz., *modes localized to radial zones underlie the*

turbulence. (Similar mode localization is suggested in an analysis of GPI data on Alcator C-Mod.[14])

The structure velocity of the separatrix-spanning mode is nearly $\langle v_{E,y}\rangle+1/2\langle v_{di,y}\rangle$ inside the separatrix, where this hybrid velocity is maximized, and corresponds to the phase (and group) velocity of an ion-diamagnetic-modified interchange mode, in the local approximation to the dispersion relation. Damping the mean vorticity, encourages $\langle v_{E,y}\rangle \rightarrow -\langle v_{di,y}\rangle$ (cf. Eq. 5) and reduces the mode velocity and the structure velocity significantly near the separatrix, as shown in Fig. 5. The flow shear rate similarly decreases with increased damping and, particularly in the pre-Li case, the heat flux (P_{SOL}) increases, suggesting that the flow shear is controlling the turbulence in pre-Li profiles. (The profiles with lithium are relatively immune to flow damping, likely because the saturation mechanism is wave-breaking as opposed to shear-stabilization.)

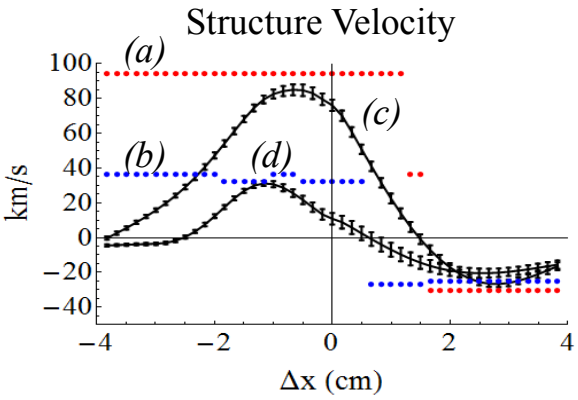

FIG. 5. The structure velocity without (a) and with (b) flow damping, constant on radial zones, reveals underlying radial eigenmodes. The flow profile $\langle v_{E,y}\rangle+\frac{1}{2}\langle v_{di,y}\rangle$ is shown for comparison: without (c) and with (d) flow damping.

5. Conclusion

SOLT simulations have been compared with lithium deposition experiments on NSTX to explore the nature of the interchange turbulence driven by experimental pressure profiles with and without lithium deposition and, in particular, the possibility that trends observed in SOL heat flux width may be attributed to turbulent transport. We find that, when simulation power (P_{SOL}) is adjusted to match that of the experiment, SOL heat-flux widths are smaller for the gentler pressure profiles that result from lithium deposition, and larger for the steeper pre-lithium profiles. This trend agrees with experiment. The apparent explanation for the trend, derived from these simulations, is that turbulent transport (blobs) generated in the lower pedestal region drives the heat flux and heat flux width in the SOL. Steeper profiles drive stronger turbulence; simulated with-Li density fluctuations measured at the separatrix are weaker across the spectrum than pre-Li fluctuations, in qualitative agreement with reflectometry measurements.

Modes localized to radial zones underlie the turbulence. The simulated structure velocity near the separatrix is approximately $\langle v_{E,y}\rangle + \frac{1}{2}\langle v_{di,y}\rangle$, as expected of interchange modes modified by ion diamagnetic effects. Flow damping reduces SOLT structure velocities, as required for agreement with GPI observations. For the flow-shear controlled turbulence of the pre-Li profiles, increased flow damping leads to stronger turbulence which drives larger P_{SOL} and heat flux widths. But with lithium deposition, the turbulence driven by the gentler profiles is relatively immune to increased flow damping. An important topic for future studies is the possible interplay between neutral recycling, flow damping by neutrals, and its impact on the heat flux width.

[1] H. W. Kugel, M. G. Bell, J.-W. Ahn, J. P. Allain, R. Bell, J. Boedo, C. Bush, D. Gates, T. Gray, S. Kaye, R. Kaita, B. LeBlanc, R. Maingi, R. Majeski, D. Mansfield, J. Menard, D.
[2] M. G. Bell, H. W. Kugel, R. Kaita, L. E. Zakharov, H. Schneider, B. P. LeBlanc, D. Mansfield, R. E. Bell, R. Maingi, S. Ding, S. M. Kaye, S. F. Paul, S. P. Gerhardt, J. M. Canik, J. C. Hosea, G. Taylor, and the NSTX Research Team, Plasma Phys. Controlled Fusion **51**, 124054 (2009).
[3] R. Maingi, T. H. Osborne, B. P. LeBlanc, R. E. Bell, J. Manickam, P. B. Snyder, J. E. Menard, D. K. Man, H. W. Kugel, R. Kaita, S. P. Gerhardt, S. A. Sabbagh, F. A. Kelly, and the NSTX Research Team, Phys. Rev. Lett. **103**, 075001 (2009).
[4] R. Maingi, D.P. Boyle, J.M. Canik, S.M. Kaye, C.H. Skinner, J.P. Allain, M.G. Bell, R.E. Bell, S.P. Gerhardt, T.K. Gray, M.A. Jaworski, R. Kaita, H.W. Kugel, B.P. LeBlanc, J. Manickam, D.K. Mansfield, J.E. Menard, T.H. Osborne, R. Raman, A.L. Roquemore, S.A. Sabbagh, P.B. Snyder and V.A. Soukhanovskii, Nucl. Fusion **52**, 083001 (2012).
[5] T.K. Gray, J.M. Canik, R. Maingi, A.G. McLean, J-W. Ahn, M.A. Jaworkski, R. Kaita, M. Ono, S.F. Paul and the NSTX Team, Nucl. Fusion **54**, 023001 (2014).
[6] J. M. Canik, R. Maingi, S. Kubota, Y. Ren R. E. Bell,3 J. D. Callen, W. Guttenfelder, H. W. Kugel, B. P. LeBlanc, T. H. Osborne, and V. A. Soukhanovskii, Phys. Plasmas **18**, 056118 (2011).
[7] J. R. Myra, D. A. Russell, D. A. D'Ippolito, J-W. Ahn, R. Maingi, R. J. Maqueda, D. P. Lundberg, D. P. Stotler, S. J. Zweben, J. Boedo, M. Umansky and NSTX Team, Phys. Plasmas **18**, 012305 (2011).
[8] D. A. Russell, D. A. D'Ippolito, J. R. Myra, B. LaBombard, J. L. Terry, and S. J. Zweben Phys. Plasmas **19**, 082311 (2009).
[9] S. I. Krasheninnikov, D. A. D'Ippolito and J. R. Myra, J. Plasma Phys. **74**, 679 (2008).
[10] A.N. Simakov and P.J. Catto, Phys. Plasmas **10**, 4744 (2003).
[11] M.V. Umansky, X.Q. Xu, B. Dudson, L.L. LoDestro and J.R. Myra, Comp. Phys. Comm. **180**, 887 (2009).
[12] S. Kubota, private communication.
[13] B. Cao, S. J. Zweben, D. P. Stotler, M. Bell, A. Diallo, S. M. Kaye and B. LeBlanc, Plasma Phys. Control. Fusion **54**, 112001 (2012).
[14] I. Cziegler, J. L. Terry, J. W. Hughes, and B. LaBombard, Phys. Plasmas **17**, 056120 (2010).